Research Inventy: International Journal of Engineering and Science
Vol.16, Issue 5 (May 2026), PP 33-40
Issn (e): 2278-4721, Issn (p):2319-6483, www.researchinventy.com

Numerical Simulation of Convective Drying Kinetics of Sweet Potato using COMSOL Multiphysics: A Multiphase Transport Approach

Ut Hien Nguyen Thi*, Van Nam Le
Faculty of Mechanical engineering and Technolofy, Ho Chi Minh City University of Industry and Trade, 140 Le Trong Tan, Tay Thanh, Ho Chi Minh City, Vietnam, 700000

Abstract: *This study presents a multiphase porous media model to simulate the heat and mass transfer during convective drying of sweet potatoes. Developed in COMSOL Multiphysics, the model couples the Brinkman and Darcy laws to analyze the interaction between temperature, relative humidity, and pore pressure. Results reveal that the internal pressure gradient, driven by phase-change evaporation, acts as the pivotal driving force for moisture expulsion, surpassing traditional diffusion mechanisms. Validation using GAB/Henderson models demonstrates high predictive accuracy. This framework provides a robust tool for optimizing industrial drying parameters, enhancing energy efficiency, and ensuring the quality preservation of agricultural products.*
Keywords: *Multiphase transport, Porous media, Sweet potato drying, Pressure gradient*

Date of Submission: 05-05-2026 Date of Acceptance: 15-05-2026

I. INTRODUCTION

Sweet potato (*Ipomoea batatas* L.) is a strategic food crop that provides an abundant source of carbohydrates, potassium, fiber, and beta-carotene, as evidenced by the studies of Babu et al. (2015), Bovell-Benjamin (2007), and Dereje et al. (2020). However, with an initial moisture content often exceeding 75%, this agricultural product is highly susceptible to microbial infestation and biochemical degradation. To address this issue, Hot Air Drying (HAD) is a widely adopted solution to reduce water activity to a safe threshold, as affirmed by Ekwere et al. (2019) and Falade & Solademi (2010). Although assisted technologies such as infrared or microwave radiation have been evolving rapidly through the works of Gasa et al. (2022), Onwude et al. (2018), and Junqueira et al. (2016), purely experimental research still faces challenges in observing internal heat and mass transfer phenomena.

Historically, semi-empirical thin-layer models such as Page, Henderson & Pabis, or Midilli—have been prioritized by Workneh & Oke (2014) and Aghabashlo et al. (2008) due to their simplicity, with the Midilli model frequently demonstrating the highest compatibility with experimental data for sweet potatoes. However, according to Turkan et al. (2019), these remain "black-box" models that fail to explain the underlying physical mechanisms within the food structure. Consequently, modern research, following the direction of Datta (2007), has shifted toward modeling sweet potato as a multiphase porous medium, where heat transfer (convection, radiation) and mass transfer (vapor diffusion, liquid capillary flow) are solved simultaneously.

To solve the system of coupled partial differential equations (PDEs) involving temperature, moisture concentration, and pressure, COMSOL Multiphysics (2021) has become a powerful numerical simulation tool. Notably, the study by Cao et al. (2023) integrated the Arbitrary Lagrangian-Eulerian (ALE) method, proving that accounting for structural shrinkage phenomena leads to more accurate predictions of drying time and actual volume changes. The utilization of these robust simulation tools allows for the resolution of mass and energy conservation equations, facilitating precise prediction of moisture and temperature distribution. This, in turn, optimizes the drying process, enhances energy efficiency, and preserves valuable bioactive compounds, as analyzed by Solomon et al. (2021).

While semi-empirical models offer high statistical compatibility, their "black-box" nature fails to elucidate the internal physical mechanisms during drying. To address this limitation, this study adopts a multiphase porous media modeling approach, enabling a detailed description of complex heat and mass transfer interactions. By utilizing the finite element method within COMSOL Multiphysics, the governing equations for mass and energy conservation are solved simultaneously. This approach ensures precise prediction of drying kinetics, providing a robust foundation for process optimization and the preservation of the essential nutritional values of sweet potatoes.

II. RESEARCH METHODOLOGY

2.1. Model Assumptions

The drying process of sweet potatoes is described based on multiphase transport theory in hygroscopic porous media. To establish the mathematical framework, the following assumptions are applied (Datta, 2007; Turkan et al., 2019):

- The sweet potato is treated as a porous medium consisting of three phases: solid (cell matrix), liquid (water), and gas (moist air).
- Local thermal equilibrium is maintained among the three phases.
- Gravitational effects are neglected due to the small sample size and the dominance of capillary forces (Halder et al., 2007).
- Gas flow within the pores follows the Brinkman equation, accounting for both Darcy resistance and viscous friction (Kumar et al., 2012).

2.2. Governing Equations

2.2.1. Moisture Transport Equation

The variation of total moisture content $\emptyset_{\omega}[\frac{Kg}{m^3}]$ over time is described by the mass conservation equation (Datta, 2007; Cao et al., 2023):

$$\frac{\partial \emptyset_{\omega}}{\partial t} + \nabla.\left(\boldsymbol{\rho_g u_g \omega_v} + \boldsymbol{g_w} + \boldsymbol{\rho_l u_l}\right) = \mathbf{0} \qquad [\mathbf{1}]$$

Where:

Vapor phase transport: Includes convection $\boldsymbol{\rho_g u_g \omega_v}$and binary diffusion $\boldsymbol{g_w = -\rho_g D_{eff} \nabla \omega_v}$

Liquid phase transport: Includes Darcy-based convection $\boldsymbol{\rho_l u_l}$ and capillary flow $\boldsymbol{g_{cl} = -D_w \nabla \emptyset_{\omega}}$

2.2.2. Heat Transfer Equation

Energy conservation is governed by the heat transfer equation in porous media, considering effective thermophysical properties and latent heat due to phase change (Aghabashlo et al., 2008):

$$(\boldsymbol{\rho C_P})_{eff} \frac{\boldsymbol{\partial T}}{\boldsymbol{\partial t}} + (\boldsymbol{\rho C_P})_{eff}.\boldsymbol{u_{eff}}.\boldsymbol{\nabla T} + \nabla.\mathbf{q} = \boldsymbol{Q_{evap}} \qquad [\mathbf{2}]$$

Where:

Effective Properties $(\boldsymbol{\rho C_P})_{eff}$: Calculated according to the mixture law (rule of mixtures) based on liquid saturation ($\boldsymbol{s_l}$) and gas saturation $\boldsymbol{s_g}$).

The evaporative heat source $\boldsymbol{Q_{evap} = L_v G_{evap}}$ represents the energy required to break moisture bonds within the sweet potato structure.

2.2.3. Flow Dynamics

Gas Phase: The Brinkman equation is used to determine the velocity field $\boldsymbol{u_g}$ and gas pressure $\boldsymbol{P_g}$

Liquid Phase: The liquid water velocity $\boldsymbol{u_l}$ is determined via the gas phase pressure gradient: (Turkan et al., 2019).$\boldsymbol{u_l = -\frac{k_l}{\mu l} \nabla P_g}$

2.3. Constitutive Relations for Sweet Potato

Sorption Isotherms: The relationship between relative humidity and equilibrium moisture content is described by GAB or Henderson models (Falade & Solademi, 2010; Workneh & Oke, 2014).

Relative Permeability: The coefficients $\boldsymbol{k_{rl}}$, $\boldsymbol{k_{rg}}$ are functions of liquid saturation $\boldsymbol{s_l}$based on empirical data for vegetables (Datta, 2007).

Diffusion Coefficients: The effective diffusion coefficient $\boldsymbol{D_{eff}}$ is determined based on pore structure and drying temperature (Ekwere et al., 2019).

2.4. Boundary Conditions and Numerical Solution

Robin boundary conditions (Type III) are applied at the interface surfaces to describe convective heat and mass exchange (Aghabashlo et al., 2008). The system of coupled equations is solved using the Finite Element Method (FEM) on the COMSOL Multiphysics 6.0 platform.

2.5. Simulation Setup

2.5.1. Geometric Model and Computational Domain

The geometry is constructed based on the actual specifications of the multi-purpose dryer at the Faculty of Mechanical Engineering, Ho Chi Minh City University of Industry and Trade.

Drying Chamber: Designed as a 3D space to simulate the hot air flow surrounding the material.

Figure 1. Parameters of the drying chamber and the drying material

a) Drying chamber **(b) Drying material**

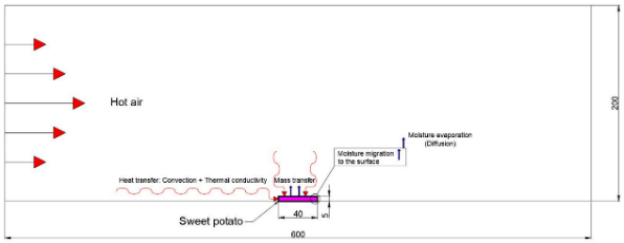

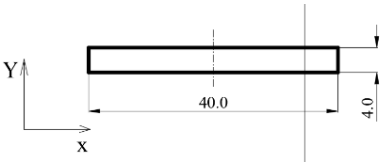

Drying Material: Sweet potato samples are modeled in COMSOL using a cylindrical geometry (Ø20 mm x 4 mm thickness). These dimensions match the experimental setup, with samples placed at fixed positions on the drying tray to investigate internal heat and moisture transfer interactions

2.5.2. Meshing and Time-Stepping Control

Mesh Type: An unstructured mesh with "Extremely Fine" resolution is employed to ensure convergence for strongly nonlinear coupled equations.

Figure 2. Meshed model of the sweet potato and drying chamber

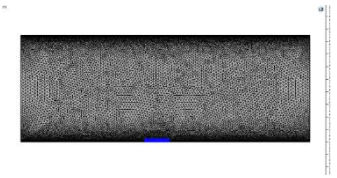

Mesh Parameters: Maximum element size is 2.15 mm, with a minimum of 0.0215 mm. The element growth rate is limited to 1.3 with a curvature factor of 0.2 to refine the mesh at boundary layers where intense heat and mass exchange occur.

Time Stepping: A fixed time step of t = 1s is utilized, selected after convergence testing to capture detailed variations in temperature and moisture without excessive computational cost.

Figure 3. Meshed view of the sweet potato sample

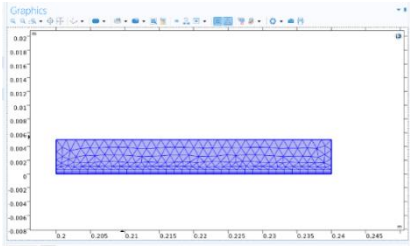

2.5.3. Selection of Probes

To monitor drying kinetics, domain and boundary probes are established at strategic locations

Surface Probes: Located at the boundary layer to monitor evaporation rates and surface temperature fluctuations.

Figure 4. Selected nodes at the surface and the center

a) Surface node **b) Center node**

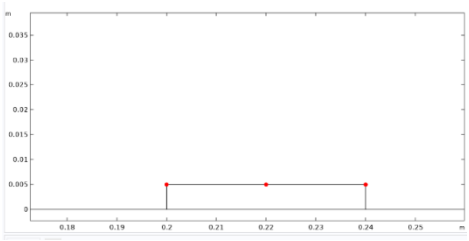

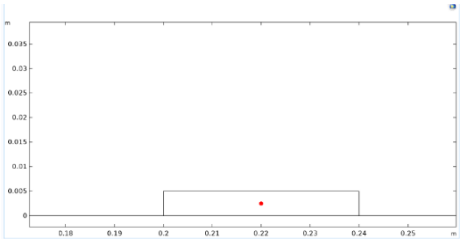

Core Probes: Placed at the geometric center of the sample to track conductive heat transfer and moisture migration from the interior.

2.5.4. Input Physical and Thermophysical Parameters

The parameters for the sweet potato, gas, and liquid phases are established based on experimental data and reliable literature.

Table 1: Key parameters used in the simulation model

Symbol	Parameter	Value	Unit
Drying Air Flow			
T_0	Drying chamber temperature	323 K	Experimental
U_0	Air velocity	0.75 m/s	Experimental
θ_0	Air relative humidity	0.26	Calculated
Drying Material			
T_1	Initial material temperature	27°C	Experimental
θ_1	Initial moisture content	0.57	Experimental
s_0	Initial liquid saturation	0.1	-
por	Porosity	0.6	Morrow (1970)
k_S	Permeability	0.49 W/mK	Farinu & Baik (2007)
C_{P0}	Specific heat capacity	3660 J/(kg·K)	Farinu & Baik (2007)
ρ_0	Density	1212 kg/m³	Farinu & Baik (2007)

III. RESULTS AND DISCUSSION

3.1. Relative Humidity Distribution

Figure 5: Distribution of internal relative humidity: a) RH field at t=10s; b) RH field at t=9000s

a) **b)**

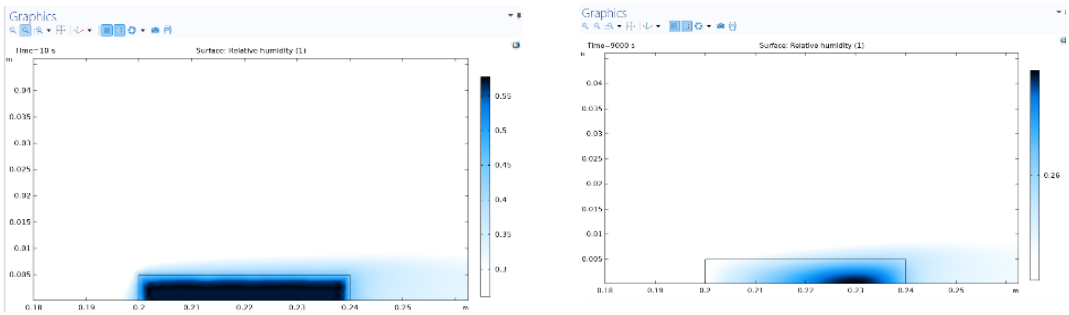

The evolution of the relative humidity (RH) field throughout the simulation period highlights the dehydration mechanism characteristic of porous media. At the initial stage (t = 10s), the material is near a fully saturated state. However, by t= 9000s, the drying front has receded deep into the core, significantly reducing the RH levels in the outer layers. This RH stratification demonstrates the continuous mass transport from the core to the surface, driven by thermal energy and internal pressure gradients

3.2. Pressure Field Distribution

Figure 6: Distribution of the pressure field: a) Pressure field at t= 10s; b) Pressure field at t= 9000s

a) **b)**

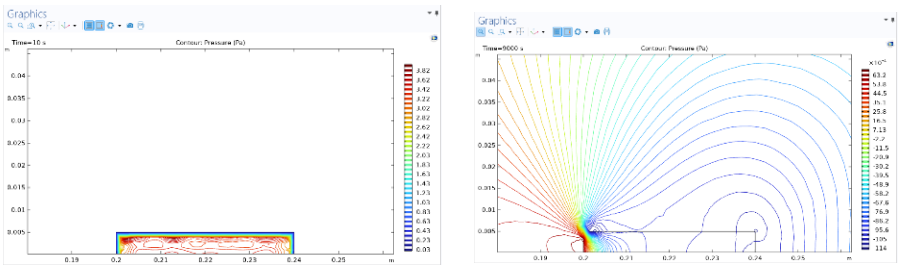

The simulation of the pressure field illustrates a significant transition in drying dynamics. At t = 10s, pressure begins to accumulate near the boundaries due to instantaneous evaporation. By t = 9000s, the isobars have propagated extensively, establishing a sustained pressure gradient. This pressure differential acts as a primary driving force for Darcy flow, facilitating more efficient moisture migration toward the surface.

3.3. Liquid Water Saturation Distribution

Figure 7: Distribution of liquid water saturation: a) Liquid saturation at t=10s; b) Liquid saturation at t=9000s

a) **b)**

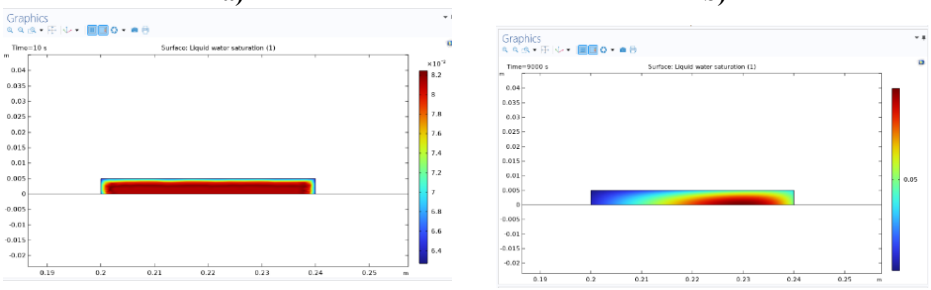

The liquid water saturation profiles provide a visual representation of the material's drying progression. At t = 10s, the entire cross-section is characterized by a deep red color, corresponding to the maximum saturation state at the onset of the drying process. By t = 9000s, the saturated (red) zone has significantly contracted and shifted toward the bottom, while the upper surfaces transition to blue, indicating low moisture levels. This observation confirms that the drying front is advancing toward the core, with liquid water being expelled toward the boundaries under the influence of pressure gradients. These results validate the moisture transport efficiency captured by the multiphase model.

3.4. Temperature Field Distribution

Figure 8: Distribution of the temperature field: a) Temperature field at =10s; b) Temperature field at t=9000s

a) **b)**

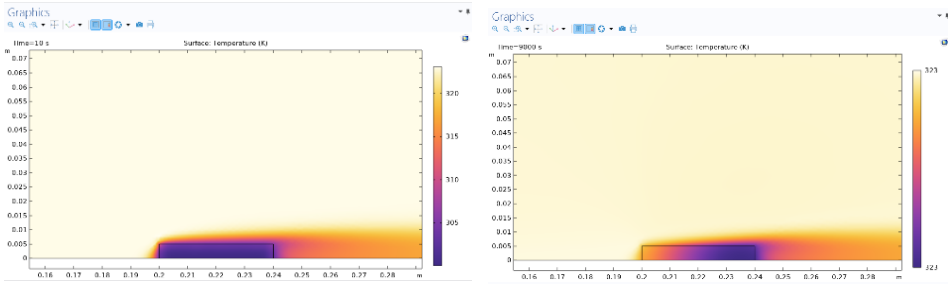

The simulation results for the temperature field at two distinct time intervals clearly illustrate the heat transfer process into the material. At t = 10s, the temperature increase is confined to the boundary layer in direct

contact with the drying agent, while the core remains at its initial low temperature (indicated by the deep purple zone). By t = 9000s, thermal energy has penetrated deep into the center, significantly contracting the low-temperature region. The shift in color gradients from orange to purple provides evidence of effective internal heat conduction and surface convection. These mechanisms provide the necessary energy to drive evaporation and generate the internal pressure required for moisture expulsion.

3.5. Temperature Evolution at Monitored Locations

Figure 9: Temperature profiles: (a) Temperature at the core; (b) Temperature at surface locations

a) **b)**

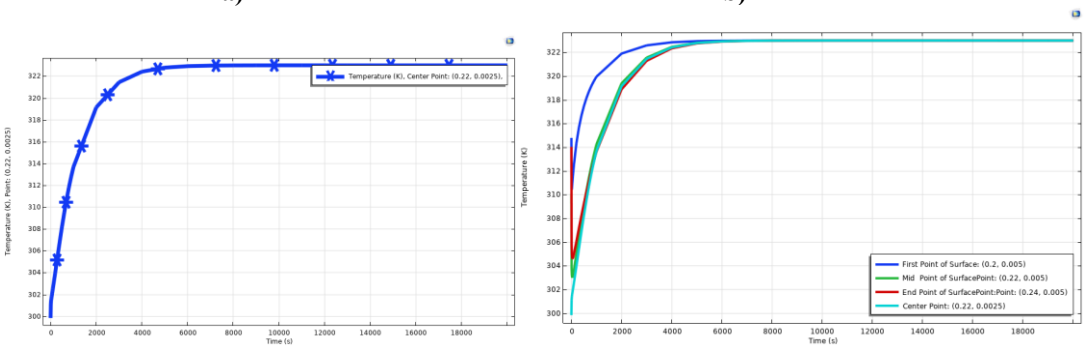

The temperature differentiation between different positions clearly reflects the internal thermal conduction resistance. During the first 2000s, the surface points undergo rapid heating, reaching approximately 320K and establishing a strong radial temperature gradient to supply the latent heat of vaporization. There is a distinct thermal lag at the core, which only converges with the surface temperature at 323K after 6000s, marking the achievement of global thermal equilibrium.

3.6. Relative Humidity (RH) Evolution at Monitored Locations

Figure10: Relative humidity profiles: (a) RH at the core; (b) RH at surface locations

a) **b)**

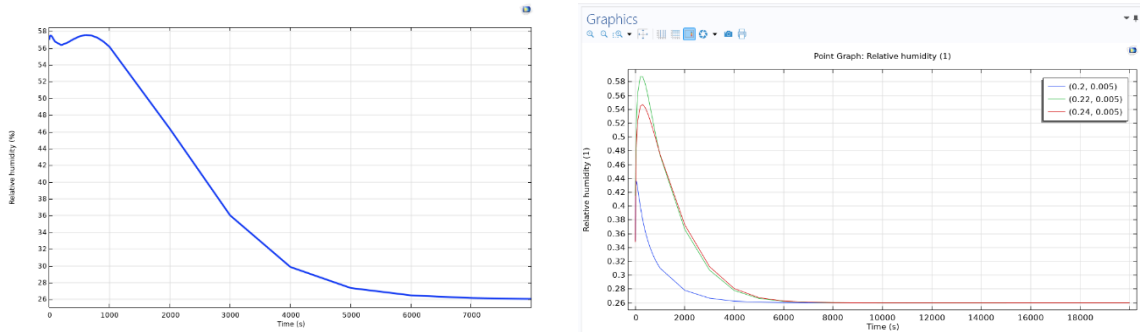

The simulation results demonstrate a strong correlation between the flow dynamics and the conservation equations. At the surface, the relative humidity (RH) exhibits significant fluctuations due to the direct impact of Robin boundary conditions and the intense evaporative heat source $\boldsymbol{Q_{evap}}$. In contrast, moisture removal at the core proceeds at a slower rate, being limited by the effective thermal conductivity ($\boldsymbol{k_{eff}}$) and effective diffusivity ($\boldsymbol{D_{eff}}$) within the porous matrix.

The convergence of all profiles toward the equilibrium level (26%) validates the accuracy of the GAB/Henderson models in describing the constitutive relations of sweet potato. The temporal discrepancy between the different points reflects the differentiation in liquid phase velocity - $\boldsymbol{k_{eff}}$) ($\boldsymbol{u_l}$ Darcy) and gas phase velocity ($\boldsymbol{u_g}$- Brinkman), proving that the mathematical model effectively resolves the coupled multiphase heat and mass transfer.

3.7. Pore Pressure Evolution at Monitored Locations

Figure 11: Pressure profiles: (a) Pressure at the core; (b) Pressure at surface locations

a) **b)**

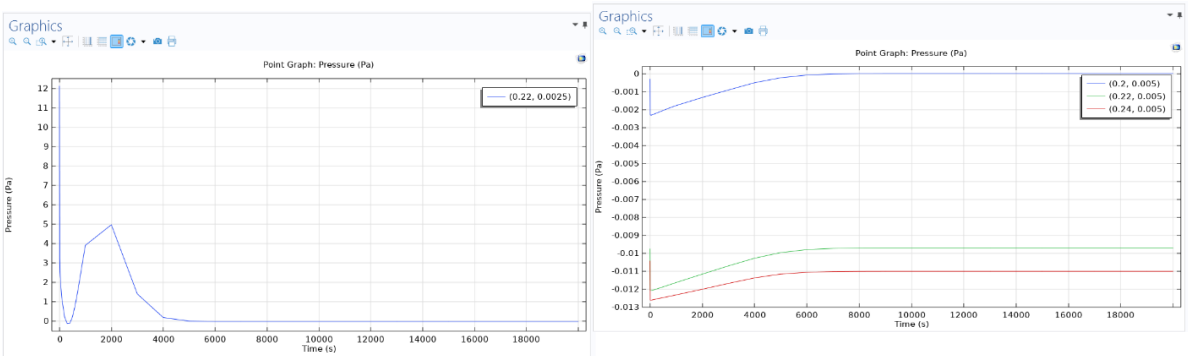

The simulation results reflect the rigorous application of the Brinkman equation and Darcy's law. At the core (a), the pressure exhibits significant fluctuations during the initial stage as internal evaporation($\boldsymbol{Q_{evap}}$) generates a positive pressure gradient. This gradient drives both the gas phase flow ($\boldsymbol{u_g}$) and liquid phase flow ($\boldsymbol{u_l}$)out of the porous structure. Conversely, at the surface (b), the pressure maintains a slight negative value and stabilizes more rapidly, reflecting the interaction with boundary conditions and instantaneous moisture release. The pressure differential between the core and the surface serves as the primary driving force for mass transport, demonstrating the tight coupling between temperature variations and pressure distribution within the model.

IV. CONCLUSION

This study successfully developed a multiphase porous media model within COMSOL Multiphysics to simulate the convective drying kinetics of sweet potatoes. The results confirm that simultaneously solving mass and energy conservation equations allows for the accurate prediction of internal heat and moisture distribution, where the pore pressure gradient serves as the pivotal driving force for moisture expulsion. The convergence of parameters toward equilibrium validates the robustness of the mathematical model and the GAB/Henderson constitutive relations. This framework provides a critical tool for optimizing industrial drying processes, contributing to enhanced energy efficiency and the maximum preservation of the product's nutritional value.

Conflict of interest

There is no conflict to disclose.

ACKNOWLEDGEMENT

The author extends their sincere thanks to Ho Chi Minh City University of Industry and Trade (HUIT) for the academic support and essential facilities provided throughout this research

REFERENCES

[1]. Aghabashlo, M., et al. (2008). Mathematical modelling of thin-layer drying of carrot. *International Journal of Food Engineering*, 4(2), 1–15.

[2]. Babu, A. S., et al. (2015). Effect of different drying methods on the physico-chemical and functional properties of sweet potato flour. *Food Chemistry*, 184, 1–7.

[3]. Bovell-Benjamin, A. C. (2007). Sweet potato: A review of its past, present, and future role in human nutrition. *Advances in Food and Nutrition Research*, 52, 1–59.

[4]. Cao, S., et al. (2023). Multiphase transport modeling of sweet potato drying with shrinkage using ALE method. *International Journal of Thermal Sciences*, 185, 108051.

[5]. COMSOL. (2021). *COMSOL Multiphysics® v. 6.0*. COMSOL AB, Stockholm, Sweden.

[6]. Datta, A. K. (2007). Porous media as a generic framework for multiphase transport in foods. *Journal of Food Engineering*, 80(1), 80–95.

[7]. Dereje, B., et al. (2020). Influence of drying methods on quality attributes of sweet potato varieties. *Journal of Food Science and Technology*, 57(1), 214–222.

[8]. Ekwere, I. U., et al. (2019). Hot air convection drying of sweet potato: Kinetics and quality. *Journal of Food Process Engineering*, 42(6), e13110.

[9]. Falade, K. O., & Solademi, O. J. (2010). Modelling of air-drying of fresh and blanched sweet potato slices. *International Journal of Food Science & Technology*, 45(2), 278–288.

[10]. Farinu, A., & Baik, O. D. (2007). Thermal properties of sweet potato with respect to moisture content and temperature. *International Journal of Food Properties*, 10(4), 745–754.

[11]. Gasa, S., et al. (2022). Advances in infrared drying of root crops: A review. *Journal of Food Engineering*, 315, 110825.

[12]. Junqueira, J. R. J., et al. (2016). Microwave-assisted drying of vegetables: Process and quality. *Food and Bioprocess Technology*, 9(1), 1–18.
[13]. Morrow, N. R. (1970). Physics and thermodynamics of capillary action in porous media. *Industrial & Engineering Chemistry*, 62(6), 32–56.
[14]. Onwude, D. I., et al. (2018). Recent advances in smart drying of agricultural produce. *Innovative Food Science & Emerging Technologies*, 48, 1–15.
[15]. Solomon, A. B., et al. (2021). Impact of drying technologies on the bioactive compounds of root and tuber crops. *Food Reviews International*, 37(1), 1–25.
[16]. Turkan, B., et al. (2019). Review on the multiphase transport models in food drying. *Journal of Food Engineering*, 243, 1–15.
[17]. Workneh, T. S., & Oke, M. O. (2014). Thin-layer drying kinetics of sweet potato slices. *International Journal of Food Science and Technology*, 49(1), 1–10.